JOURNAL OF MAGNETIC RESONANCE, Series A **123,** 95–104 (1996)
ARTICLE NO. 0218

Effect of Paramagnetic Ions on NMR Relaxation of Fluids at Solid Surfaces

I. FOLEY, S. A. FAROOQUI, AND R. L. KLEINBERG*

Schlumberger–Doll Research, Ridgefield, Connecticut 06877

Received July 5, 1996

Proton NMR longitudinal and transverse relaxation times of water-saturated powder packs have been measured. The powders were a series of synthetic calcium silicates with known concentrations of iron or manganese paramagnetic ions. The rate of water proton relaxation has been found to be linearly proportional to the concentration of paramagnetic ion. The constant of proportionality is used to determine the electron relaxation time of ions at the fluid–solid interface. A substantial relaxivity is found in the absence of paramagnetic ions. Thus the oxide surface itself is an unexpectedly good relaxer of fluid-borne nuclear spins. The results answer some long-standing questions connected with the NMR properties of fluid-saturated sedimentary rocks.

INTRODUCTION

The nuclear-magnetic-resonance properties of fluids in porous media are determined to a large extent by the interactions which occur at the pore–grain interface. It has long been known that longitudinal and transverse magnetic relaxation rates of nuclei resident in gas or liquid molecules are enhanced in the presence of high-surface-area media (*1*).

Korringa, Seevers, and Torrey (*2*) provided a phenomenological outline of the nature of NMR relaxation of fluids at solid surfaces. In their model, fluid molecules diffuse to and are temporarily adsorbed by a surface. The surface consists of two types of adsorption sites, one nonmagnetic and the other magnetic. The contributions of the magnetic and nonmagnetic sites are weighted by their relative abundance, and by the respective relaxation rates of the adsorbed molecule. The bulk relaxation of the fluid operates in parallel.

One case of interest is that of the solid in which there is a low concentration of paramagnetic impurities which, due to the strong coupling between the electron and nuclear magnetic moments, dominate the relaxation rate. Kleinberg, Kenyon, and Mitra (*3*) examined the electron–nuclear interaction at the surface in some detail, pointing out how it was composed of scalar and dipolar contributions; the latter can be partially averaged away by a molecular rotation which is not hindered by the presence of the surface. They also extended the theory of Korringa *et al.* to the transverse relaxation rate, $1/T_2$. In doing so, they had to explicitly handle the question of the residence time of temporarily adsorbed fluid molecules.

Natural sedimentary rocks are a particularly challenging group of materials to which to apply these theories. These rocks are generally composed of grains, which are cemented together as a result of burial at elevated temperature and pressure over an extended period of time. Nonetheless, the pore space can account for as much as 30% of the volume. A small piece of rock that appears homogeneous to the eye usually contains diverse minerals which make up the grains, or are overgrowths on the grains. The paramagnetic ion content of rocks varies widely, but is frequently in the range of a few tenths of a percent to a few percent, almost all of that being iron (*4*).

Clay minerals, which are common constituents of sandstones, are lamellar minerals which have very large surface areas, with which considerable pore water can be intimately associated. Clay completely dominates measurements of the internal surface area of soils and rocks (*5*). However, clay appears not to play a major role in determining the surface-mediated NMR relaxation rates of rocks (*6*).

Despite the difficulties of characterizing rock materials, there have been considerable efforts made in recent years to understand the NMR properties of fluids in them. It has been found that a number of rock properties of practical interest are correlated with NMR amplitude and relaxation time. These include porosity, pore-size distribution, hydraulic permeability, and the identity of pore fluids (*7, 8*). As a result of those laboratory studies, novel ''inside-out'' NMR instruments have been built and are used in oil exploration (*8–10*).

The purpose of this work is to better understand the mechanisms that control the NMR properties of porous rocks. To that end we have synthesized granular oxides with known chemical compositions, have fully characterized their surface geometries, and have measured longitudinal and trans-

* To whom correspondence should be addressed.

1064-1858/96 $18.00

verse relaxation times of their water-saturated powder packs. These materials are similar, although not identical, to natural rocks. The most important difference is that they are free of clays and other high-surface-area minerals. Surprisingly, their NMR properties have proved to be rather similar to those of sandstones. The results provide important and useful insights into rock properties, and resolve some long-standing petrophysical questions.

THEORY

NMR relaxation rates of fluids in many porous media are strongly influenced by the fluid–solid interaction (*1, 11*). Fluid molecules diffuse, eventually reaching a grain surface where there is a finite probability that they are relaxed. The rate-limiting step can either be the relaxation process at the surface or the rate at which unrelaxed spins can be transported to the surface (*12*).

If the rate-limiting step is relaxation at the surface, the rate of magnetization decay in an individual pore is monoexponential and depends on the surface-to-volume ratio but not the pore shape. This is referred to as the ''fast-diffusion'' or ''surface-limited'' regime. In the opposite case, magnetic relaxation occurs at the grain surface but the decay of macroscopic magnetization is controlled by the transport of molecules to the surface. This is likely to be the case when pores are relatively large and/or surface relaxation is strong. This is called the ''slow-diffusion'' or ''diffusion-limited'' regime. In this regime there is a time-dependent, spatially nonuniform distribution of magnetization in the pore. This gives rise to a magnetization decay which even in a single pore has multiexponential character, and which depends on the shape of the pore.

In the diffusion-limited case, relaxation times are inversely proportional to the diffusion coefficient of the liquid. Thus diffusion-limited relaxation is characterized by a strong temperature dependence of the relaxation times. NMR relaxation of water in sedimentary rocks is only weakly dependent on temperature over the range studied (*13*), thus indicating that the relaxation must be surface limited. As we shall see, the same is true of the artificial materials which are the subject of this study.

The Korringa, Seevers, and Torrey theory (*2*) is a surface-limited theory, and therefore serves as a starting point for understanding our results. In their theory, the observed longitudinal relaxation time is given by

$$\frac{1}{T_1} = \left(\frac{1}{T_{1B}}\right) + \left(\frac{N_N}{N}\frac{1}{T_{1N} + \tau_N}\right) + \left(\frac{N_M}{N}\frac{1}{T_{1M} + \tau_M}\right). \quad [1]$$

Here T_{1B} is the relaxation time of the liquid in bulk, T_{1N} is the relaxation time of a liquid molecule coordinated to a nonmagnetic site on the solid surface, T_{1M} is the relaxation time of a liquid molecule coordinated to a magnetic site on the surface, and τ_N and τ_M are the residence times of a liquid molecule at nonmagnetic and magnetic surface sites, respectively. N is the total number of fluid molecules in the pore, N_N and N_M are the number of nonmagnetic and magnetic surface sites, respectively, and $N_N + N_M$ is assumed to be small compared to N.

While N_M may be very much smaller than N_N, the strong magnetic interaction between a paramagnetic spin and a nearby nucleus usually leads to a large value of $1/T_{1M}$. Thus paramagnetic ions on the surface can dominate the relaxation of fluid protons even if they are dilute. Both the bulk relaxation of water and its residence time on a solid surface have a strong dependence on temperature so, in the absence of temperature dependence, T_{1B} can be neglected (although it is simple to take into account in data reduction in any event), and T_{1M} satisfies the inequalities

$$T_{1N} \gg T_{1M} \gg \tau_M. \quad [2]$$

Therefore

$$\frac{1}{T_1} = \left(\frac{Sh}{V}\right)\left(\frac{n_M}{T_{1M}}\right) = \rho_1\left(\frac{S}{V}\right)_{pore}. \quad [3]$$

S and V are the surface area and volume of the pore, h is the thickness of a monolayer of water, and n_M is the proportion of surface sites occupied by paramagnetic metal ions. All material constants are included in the surface relaxivity parameter ρ_1.

The lack of temperature dependence has the further effect of allowing a simplification of the theory of transverse relaxation (*3*), which was not discussed by Korringa, Seevers, and Torrey:

$$\frac{1}{T_2} = \left(\frac{Sh}{V}\right)\left(\frac{n_M}{T_{2M}}\right) = \rho_2\left(\frac{S}{V}\right)_{pore}. \quad [4]$$

The symbols are analogous to those of Eq. [3].

The surface relaxation times T_{1M} and T_{2M} are determined by the microscopic interaction between a nuclear spin on a fluid molecule and the electron spin of a paramagnetic ion on the solid surface (*3, 14*),

$$\frac{1}{T_{1M}} = \left(\frac{\alpha A_d}{\hbar}\right)^2 \frac{S(S+1)}{15} \times \left[\frac{6\tau_{c1}}{1 + (\omega_I\tau_{c1})^2} + \frac{14\tau_{c2}}{1 + (\omega_S\tau_{c2})^2}\right] + \left(\frac{A_s}{\hbar}\right)^2 \frac{S(S+1)}{3}\left[\frac{2\tau_{c2}}{1 + (\omega_S\tau_{c2})^2}\right] \quad [5]$$

and

$$\frac{1}{T_{2M}} = \left(\frac{\alpha A_d}{\hbar}\right)^2 \frac{S(S+1)}{15} \times \left[4\tau_{c1} + \frac{3\tau_{c1}}{1+(\omega_I\tau_{c1})^2} + \frac{13\tau_{c2}}{1+(\omega_S\tau_{c2})^2}\right] + \left(\frac{A_s}{\hbar}\right)^2 \frac{S(S+1)}{3}\left[\tau_{c1} + \frac{\tau_{c2}}{1+(\omega_S\tau_{c2})^2}\right], \quad [6]$$

where

$$A_d = \frac{\gamma_I\gamma_S\hbar^2}{r^3}. \quad [7]$$

A_d and A_s are the dipolar and scalar coupling constants, and α is a factor that accounts for anisotropic motion of the adsorbed molecule (*3*). S is the electron spin, ω_I and ω_S are the Larmor frequencies of the nucleus and electron, γ_I and γ_S are the gyromagnetic ratios of the nucleus and electron, and r is the distance between the electron and nucleus during the interaction. The correlation times are

$$\frac{1}{\tau_{c1}} = \frac{1}{\tau_M} + \frac{1}{\tau_{s1}} \quad [8]$$

and

$$\frac{1}{\tau_{c2}} = \frac{1}{\tau_M} + \frac{1}{\tau_{s2}}. \quad [9]$$

τ_M is the residence time of water at a magnetic surface site, and τ_{s1} and τ_{s2} are the longitudinal and transverse relaxation times of the electron. When the relaxation rates are temperature independent, $1/\tau_M$ cannot be significant, and τ_{s1} and τ_{s2} must not depend on temperature over the range investigated.

A number of factors can make the theory more complicated. Commonly, magnetic ions have g factors that deviate significantly from the free-electron value of 2.0023, and that are anisotropic. However, since Fe^{3+} and Mn^{2+} have spin $S = \frac{5}{2}$, their g factors are normally isotropic and close to the free-electron value (*15*). Therefore $\gamma_S/\gamma_I = \omega_S/\omega_I = 658$. We neglect the possible consequences of zero-field splitting (*15*), which we have no way to assess for the ions at the fluid–solid interface.

Equations [5] and [6] are valid when the electron longitudinal and transverse magnetization decays are simple exponential functions of time. If this is not true, the terms containing τ_{s1} and τ_{s2} must be generalized. We anticipate that this may be the case (*16*), but the simple model is adequate for describing the data presented here.

These equations are more readily compared to experimental data when A_s is eliminated from the equations. We observe that when $\omega_I\tau_{c1} \ll 1$, and $\omega_s\tau_{c2} \gg 1$ or $\tau_{c1} \gg \tau_{c2}$ (which are tested below), the ratio $A_s/\alpha A_d$ can be determined from T_{1M}/T_{2M}:

$$\frac{T_{1M}}{T_{2M}} = \frac{7}{6} + \frac{5}{6}\left(\frac{A_s}{\alpha A_d}\right)^2. \quad [10]$$

This theory predicts that the observed longitudinal and transverse relaxation rates of fluid in a porous medium will be linearly proportional to the concentration of paramagnetic ions at the solid surface. The constants of proportionality will depend on the thickness of the relaxing layer, the electron relaxation times, the electron–nuclear distance, the scalar coupling constant, and the rotational anisotropy factor α.

PREVIOUS DETERMINATIONS OF SURFACE RELAXIVITY

A number of studies have been made of the relaxivity of solid surfaces in contact with fluids. Most frequently, the fluid has been water. The measurement of relaxivity requires a measurement of NMR relaxation time (T_1 or T_2), and a measurement of pore space surface-to-volume ratio. Artificial packings of uniformly sized grains produce narrow pore-size distributions. Such porous media are generally characterized by single-exponential magnetization decays and a single surface-to-volume ratio which characterizes the entire sample (*17, 18*). Various methods of measuring S/V produce consistent results. In imperfect packings, if diffusion allows fluid molecules to visit pores of different sizes during the relaxation time, a distribution of pore sizes can be averaged, resulting in a single-exponential decay (*19*). This situation is most likely to occur in well-mixed synthetic materials, but is unlikely in natural porous materials such as rocks (*20*). The results of studies of artificial packings are tabulated in Ref. (*6*); the longitudinal relaxivity ρ_1 has been reported to be in the range 1–13 μm/s for a variety of materials. In a recent study (*21*), calcium carbonate and silica were modified by deposition of iron and manganese from solution, and ρ_1 at 10 MHz was found to vary between 1 and 22 μm/s, generally increasing with paramagnetic ion content.

MATERIALS

The powders used were calcium silicates ($CaSiO_3$) in the alpha (pseudowollastonite) crystallographic phase. Pseudowollastonite was used because (1) unlike other cementitious materials, it is not hydratable; (2) Fe_2O_3 and MnO form

solid solutions with it over very wide ranges of concentrations, which allow the ions to exist in their desired oxidation states: iron as Fe^{3+} and manganese as Mn^{2+}; (3) the oxide surface is a reasonable (although not exact) analogue of the silica surface commonly found in rocks; and (4) the synthesis is well known.

Each sample was synthesized with a known concentration of either iron or manganese (Construction Technology Laboratories, Skokie, Illinois). Solid calcium silicate hydrate was mixed with aqueous solutions of Fe^{3+} and Mn^{2+} and then dehydrated at 1400°C to form the doped pseudowollastonite. The manganese and iron series were prepared from different batches of starting materials. The iron materials were fired in an oxygen atmosphere to ensure formation of Fe_2O_3 while the manganese materials were fired in a nitrogen atmosphere to prevent formation of Mn_2O_3.

The range of iron and manganese concentrations used in this investigation is coincident with concentrations found in many sandstones and carbonates (*4*), but excluding those rocks which contain large amounts of iron-rich minerals such as siderite, magnetite, chlorite, or glauconite, or manganese-rich minerals such as rhodochrosite.

The pseudowollastonite was received in the form of millimeter-sized chunks. The material was friable and was readily reduced to a very fine powder. Gentle grinding followed by sieving produced powders in the ranges 10–106 and 106–150 μm. The material was white, tending to tan with higher concentrations of iron. The purest material we obtained, 85 ppm Fe and 2 ppm Mn, had a distinct bluish tinge before being ground. The ions at the grain surfaces are expected to be oxidized to Fe^{3+} and Mn^{2+} as a result of their contact with air and water.

Upon grinding, it was discovered that there was a small proportion of reddish-brown to black specks in the materials with the higher iron concentrations. Energy-dispersive X-ray (EDX) spectroscopy revealed that these specks had elevated concentrations of iron. A magnetic separator removed these particles to the maximum extent possible.

MATERIAL CHARACTERIZATION

A number of methods were used to measure the concentration of paramagnetic ions. Inductively coupled plasma (ICP) spectrometry (XRAL Laboratories, Don Mills, Ontario) found iron and manganese concentrations consistent with that expected from the starting materials. No other magnetic ions were found above trace levels.

Magnetic susceptibility was measured with a force balance. The balance was calibrated with powder calibration samples covering a wide range of magnetic susceptibilities. The measured cgs gram susceptibility was converted to (dimensionless) SI volumetric susceptibility,

$$\chi_v(\mathrm{SI}) = 4\pi\chi_v(\mathrm{cgs}) = 4\pi\rho_{\mathrm{CaSiO_3}}\chi_g(\mathrm{cgs}), \qquad [11]$$

where $\rho_{\mathrm{CaSiO_3}}$ is the density of the powder.

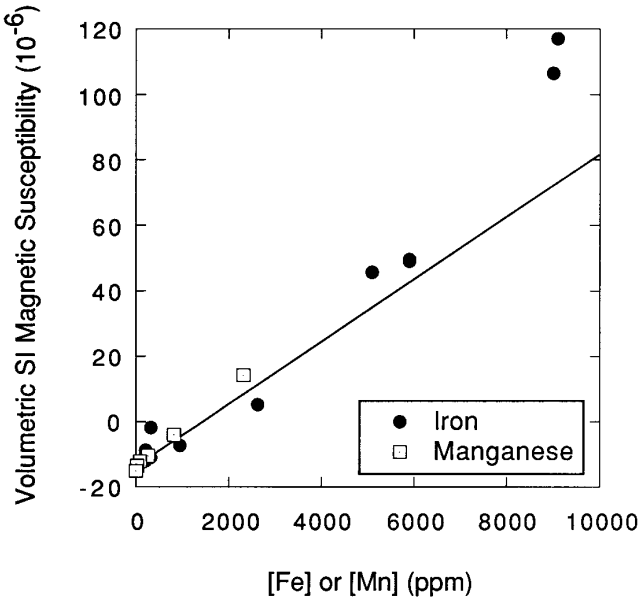

FIG. 1. Volumetric magnetic susceptibility versus concentrations (by weight) of iron and manganese as determined by ICP analysis. The straight line is the Curie law prediction, with no adjustable parameters. The zero intercept is the expected susceptibility of undoped $CaSiO_3$.

The Curie law in SI units is

$$\chi_v = \frac{n_v \mu_0 n_B^2 \mu_B^2}{3kT}, \qquad [12]$$

where n_v is the number of ions per cubic meter; $\mu_0 = 4\pi \times 10^{-7}$ H/m; μ_B is the Bohr magneton, 9.27×10^{-24} A·m^2; $n_B\mu_B$ is the magnetic moment of the ion; k is Boltzmann's constant, 1.38×10^{-23} J/K; and T is the absolute temperature. For both Fe^{3+} and Mn^{2+} the magnetic moment is 5.9 Bohr magnetons (*22*).

The number of ions of metal M per unit volume, n_v, is related to the concentration of M in parts per million by weight, $[M]_{\mathrm{ppm}}$ through

$$n_v = \frac{[M]_{\mathrm{ppm}}}{10^6} \frac{\rho_{\mathrm{CaSiO_3}}}{\mathrm{MW_M}} A, \qquad [13]$$

where $\rho_{\mathrm{CaSiO_3}}$ is the density of the solid (*23*), 2905 kg/m^3 (almost unaffected by the presence of the small concentrations of metal used in these experiments); $\mathrm{MW_M}$ is the atomic weight of the metal (kg/mol); and A is Avogadro's number, 6.02×10^{23} mol^{-1}. For iron $n_v = [\mathrm{Fe}]_{\mathrm{ppm}} \times 3.13 \times 10^{22}$ ions/m^3. The corresponding value for manganese is 2% higher.

The computed slopes $\Delta\chi_v/\Delta[M]_{\mathrm{ppm}}$ for the iron and manganese pseudowollastonites are shown in Fig. 1. The commonality of magnetic moment and atomic weight allows a

single line to represent the predicted values for both ions. There is a positive deviation from linearity at large [Fe]. The zero-concentration intercept is an estimate of the magnetic susceptibility of pure $CaSiO_3$, the average of the volume susceptibilities of CaO and SiO_2 (*23*): $\chi_v(\mathrm{SI}) = -13.7 \times 10^{-6}$.

Accurate determination of surface area is of principal importance in this investigation. The specific surface areas of all samples were measured by the BET technique (*24*). Surprisingly, the various sieved fractions showed only minor differences in surface area, all determinations of which were in the range 0.6–1.7 m^2/g. Examination of the powders in a scanning electron microscope revealed why there is no consistent difference in the surface area per gram for powders that were sieved into distinct particle size fractions. Each particle appeared to be composed of lightly sintered microparticles having a characteristic size around 1 μm. This finding explains the friability of the starting material. It also explains why all size fractions had BET surface areas of around 1 m^2/g, which corresponds to an equivalent particle radius of 1 μm:

$$r = \frac{3}{\rho_{\mathrm{CaSiO_3}} S_{\mathrm{BET}}}. \qquad [14]$$

In this equation, $\rho_{\mathrm{CaSiO_3}}$ is the density of the powder and S_{BET} is the surface area per unit mass.

SAMPLE PREPARATION

To make a water-saturated sample, an excess of degassed water was thoroughly mixed with a weighed amount of powder in a weighed sample tube. The sample was sonicated to remove bubbles and then packed by being briefly centrifuged. The supernatant liquid was decanted, and a final weight was obtained; the weight of water was obtained by difference. To minimize any possible alteration of the samples by dissolution or hydration of the solid, each sample was prepared immediately before NMR measurements, and dried immediately afterward in a 70°C oven.

NMR CHARACTERIZATION

All proton NMR measurements were made at a frequency of 2 MHz. This is the frequency at which many rock measurements have been made, and it is in the frequency range of the borehole NMR instruments (*8*). The principal advantage of 2 MHz measurements is that the transverse surface relaxivity is usually not masked by the diffusion of water in the internal magnetic field gradients of the porous media.

Longitudinal relaxation was measured by the echo-detected inversion-recovery technique

$$\{[W\text{—}180°\text{—}\mathrm{tr}_j\text{—}(90°)_{\pm}\text{—}\mathrm{TE}/2\text{—} (180°\text{—}\mathrm{TE}/2\text{—}\mathrm{echo}_i\text{—}\mathrm{TE}/2)_i]_j\}_k. \qquad [15]$$

At each recovery time, $i = 100$ echoes were acquired, the first eight of which were averaged for subsequent processing; the echo spacing TE = 0.16 ms; the wait time $W = 10$ s; $j = 29$ recovery times, tr, were employed. They were logarithmically spaced, six per decade, ranging from 0.08 to 3710 ms. Phase alternation of the 90° pulse was used to null offsets (*25*); the measurements were stacked $k = 2 \times 10$ times, the resulting signal-to-noise ratio being about 50:1. Total measurement time was approximately 2 hours for each sample.

Transverse relaxation times were measured using the CPMG sequence

$$[W\text{—}(90°)_{\pm}\text{—}\mathrm{TE}/2\text{—} (180°\text{—}\mathrm{TE}/2\text{—}\mathrm{echo}_i\text{—}\mathrm{TE}/2)_i]_k. \qquad [16]$$

$i = 4095$ echoes were detected, with echo spacing TE = 0.16 ms. The wait time $W = 5$ s. Phase alternation of the 90° pulse was used to null offsets; the measurements were stacked $k = 2 \times 40$ times, the resulting signal-to-noise ratio being about 100:1. Total measurement time was approximately 7 minutes for each sample.

Porous media can have broad distributions of pore sizes. For example, mercury injection porosimetry of natural rock reveals that pore openings range over several orders of magnitude (*26*). In such materials, nuclear-magnetic-resonance magnetization decays are nonexponential and may be characterized by a sum of exponential decays (*27*). For longitudinal relaxation measured by inversion recovery,

$$M(t) = \sum_i m_i \left[1 - 2\exp\left(-\frac{t}{T_{1i}}\right)\right], \qquad [17]$$

and for transverse relaxation,

$$M(t) = \sum_i m_i \exp\left(-\frac{t}{T_{2i}}\right). \qquad [18]$$

In these equations, the m_i are proportional to volumes of fluid relaxing at rates $1/T_{1i}$ and $1/T_{2i}$, respectively. In water-saturated samples in which relaxation at grain surfaces is the dominant mechanism of longitudinal and transverse relaxation, the relaxation times are

$$\frac{1}{T_{1i}} = \rho_1\left(\frac{S}{V}\right)_i \qquad [19]$$

and

$$\frac{1}{T_{2i}} = \rho_2\left(\frac{S}{V}\right)_i, \qquad [20]$$

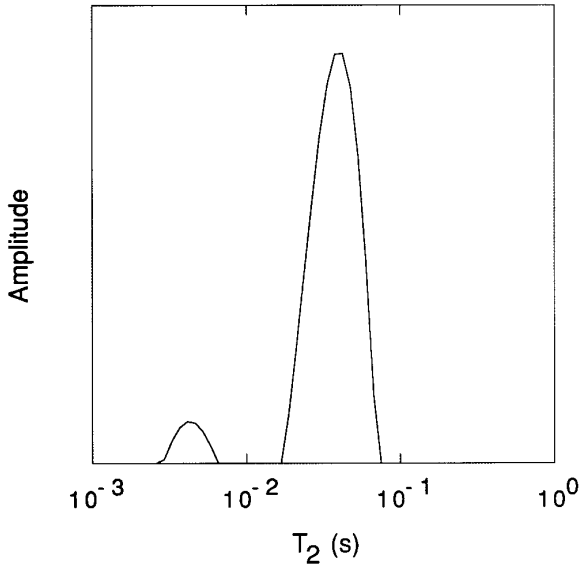

FIG. 2. The T_2 distribution for water-saturated calcium silicate powder, [Fe] = 9000 ppm. The main peak is consistent with monoexponential decay, given the signal-to-noise ratio of the data and the processing algorithm used. The satellite peak is due to a visible layer of fine powder at the top of the sample, and is disregarded in the computation of the relaxivity.

where $(S/V)_i$ is the surface-to-volume ratio of pores relaxing at rates $1/T_{1i}$ and $1/T_{2i}$, respectively.

Determination of the values of m_i is difficult. The decomposition of a magnetization decay into a sum of exponentials is an ill-posed problem, in the mathematical sense, and is nontrivial. However, there are now a number of techniques (*28–30*) which use regularization to obtain stable, reproducible distributions of m_i. We have used one such technique to analyze our data (*31*). Regularization tends to artificially broaden relaxation time distributions. The extent of the broadening depends on the number of data points and the signal-to-noise ratio.

A typical example of the relaxation time distributions obtained in this investigation is shown in Fig. 2. There is a small satellite to the left of the main peak, which is a result of the sample-preparation method. Each powder pack was stirred in degassed water until no more bubbles were visible and then centrifuged. Particles clouding the supernatant liquid settled in a thin layer on top. This layer, which was visibly different, has smaller pores than the main body of the pack. When the thin top layer was removed and the sample remeasured, the satellite peak disappeared. Satellite peaks never represented more than a few percent of the signal.

The main peaks of the transverse relaxation distributions were typically a third of a decade wide at half-maximum. The longitudinal relaxation data typically produced somewhat wider main peaks due to the much smaller number of time samples. The widths of the main peaks are consistent with those found by measurement and simulation of NMR relaxation of water in packs of mono-sized glass beads (*32*). The glass beads also occasionally display satellite peaks, which are signal-processing artifacts. In the present work, the relaxation time at the center of the main peak was used to compute the relaxivity.

The stretched exponential function is also a way of characterizing nonexponential decays (*33*):

$$M(t) = M_0\left\{1 - 2\exp\left[-\left(\frac{t}{T_{1\alpha}}\right)^{\alpha 1}\right]\right\} \qquad [21]$$

$$M(t) = M_0\exp\left[-\left(\frac{t}{T_{2\alpha}}\right)^{\alpha 2}\right]. \qquad [22]$$

When $\alpha = 1$, the decay is monoexponential.

In order to quantify how well the decays could be represented by single exponentials, the data were also analyzed as stretched-exponential decays. Except for a few cases, α_1 and α_2 are near unity, indicating predominantly single-exponential character. The data included the signal from the thin layer of fine powder at the top of the sample. Relaxation times determined from the stretched-exponential analysis and from the main peak of the corresponding distribution typically differed by a few percent.

TEMPERATURE DEPENDENCE OF THE RELAXATION TIMES

Two samples were chosen to study the temperature dependence of the relaxation times. One contained about 1% Fe and the other less than 200 ppm Fe. Unlike the room-temperature measurements, which were performed in a conventional NMR apparatus, the measurements at elevated temperatures were performed using an ''inside-out'' NMR apparatus, where the sample is external to the magnets and radiofrequency antenna (*10*). The Larmor frequency was approximately 2 MHz.

The apparatus described by Latour *et al.* (*13*) was used to thermostat the samples. A hot-air flow loop regulated the temperature to within 0.2°C between 25 and 175°C. All construction materials were nonmetallic, completely free of a discernible hydrogen signal over the entire temperature range of interest, and dimensionally stable. There were no shifts in sensitivity as the samples were heated. The temperature of the magnets and the antenna was stabilized at 35°C; the surface temperature of the antenna varied by less than 1°C and the rest of the assembly varied even less.

The samples were sealed inside a pressure vessel consisting of a ceramic cylinder and two threaded ceramic end caps. A piston seal was formed on the walls of the cylinder by Viton O-rings, trapping any vapor inside the vessel. The vessel was capable of withstanding 1.5 MPa (225 psi), the

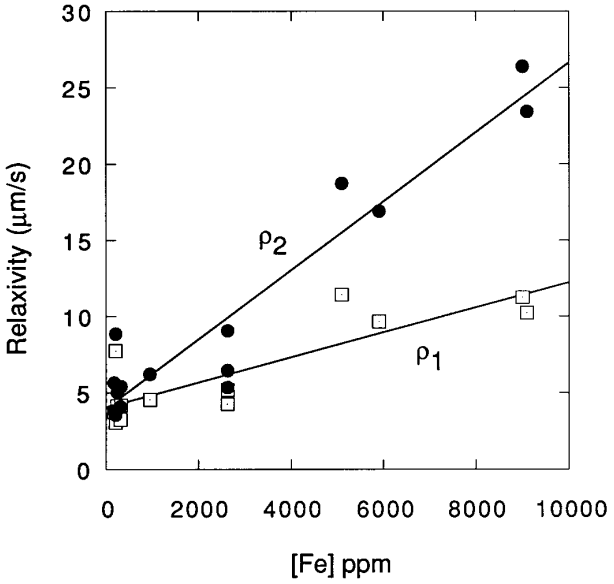

FIG. 3. Longitudinal (open squares) and transverse (solid circles) surface relaxivities for the iron-doped materials. The straight lines are least-squares fits to the data.

vapor pressure of water at 200°C. A small air space allowed for the thermal expansion of the liquid, which otherwise could have broken the vessel. The ceramic and O-rings had no NMR signal under measurement conditions. Thermometer probes were taped to the outside surface of the ceramic vessel. A half hour was sufficient for the temperature of the pressure vessel to stabilize after each temperature change.

The temperature was increased in steps from 25 to 175°C. The signal amplitude obeyed the Curie law, indicating that no water was lost as a result of heating. After the measurement at 175°C, the sample was allowed to cool back to room temperature and the initial measurement was repeated. A comparison of the signal amplitudes from the first and last measurements additionally verified that there was no loss of water from the sample.

RESULTS

Values of surface relaxivities ρ_1 and ρ_2 for each sample were determined from BET measurements of surface area per unit mass, S_{BET}, the mass of the powder, M_s, the volume of water, V_w, the bulk-water relaxation times, $T_{1\mathrm{B}}$ and $T_{2\mathrm{B}}$, and the relaxation times at the maxima of the relaxation time distributions, $T_{1,\mathrm{peak}}$ and $T_{2,\mathrm{peak}}$:

$$\rho_{(1,2)} = \frac{T_{(1,2)\mathrm{B}} - T_{(1,2)\mathrm{peak}}}{T_{(1,2)\mathrm{B}} T_{(1,2)\mathrm{peak}}} \frac{V_w}{S_{\mathrm{BET}} M_s}. \qquad [23]$$

Resulting values of ρ_1 and ρ_2 are plotted against iron and manganese concentrations in Figs. 3 and 4. For at least the iron materials, the NMR measurements probably do not contribute to the scatter, since the T_1/T_2 ratios vary smoothly with composition, as shown below. We believe that the scatter is primarily due to uncertainties in the determination of the water volume. The reduced scatter in the manganese data can be attributed to experience gained in sample preparation, as these samples were measured last.

In all cases, the data are adequately described by a linear dependence of relaxivity on paramagnetic concentration, as predicted by theory:

$$\begin{aligned}
\rho_1 &= 4.05\ \mu\mathrm{m/s} + (0.000819\ \mu\mathrm{m/s/ppm})\,[\mathrm{Fe}]_{\mathrm{ppm}} \\
\rho_2 &= 3.96\ \mu\mathrm{m/s} + (0.00227\ \mu\mathrm{m/s/ppm})\,[\mathrm{Fe}]_{\mathrm{ppm}} \\
\rho_1 &= 0.406\ \mu\mathrm{m/s} + (0.000919\ \mu\mathrm{m/s/ppm})\,[\mathrm{Mn}]_{\mathrm{ppm}} \\
\rho_2 &= 2.01\ \mu\mathrm{m/s} + (0.00106\ \mu\mathrm{m/s/ppm})\,[\mathrm{Mn}]_{\mathrm{ppm}}, \qquad [24]
\end{aligned}$$

where the concentration of metal ion is measured in weight ppm. The quantity n_{M} used in Eqs. [3] and [4] is the fractional composition. To convert from ppm by weight to fractional composition, we employ the conversion

$$n_{\mathrm{M}} = \frac{[M]_{\mathrm{ppm}}}{10^6} \frac{\mathrm{MW}_{\mathrm{CaSiO_3}}}{\mathrm{MW}_{\mathrm{M}}}, \qquad [25]$$

where $\mathrm{MW}_{\mathrm{CaSiO_3}}$ is the formula weight of calcium silicate and MW_{M} is the formula weight of the metal ion. $[M]_{\mathrm{ppm}} = 4.81 \times 10^5 \cdot n_{\mathrm{Fe}}$ for iron and $4.72 \times 10^5 \cdot n_{\mathrm{Mn}}$ for manganese.

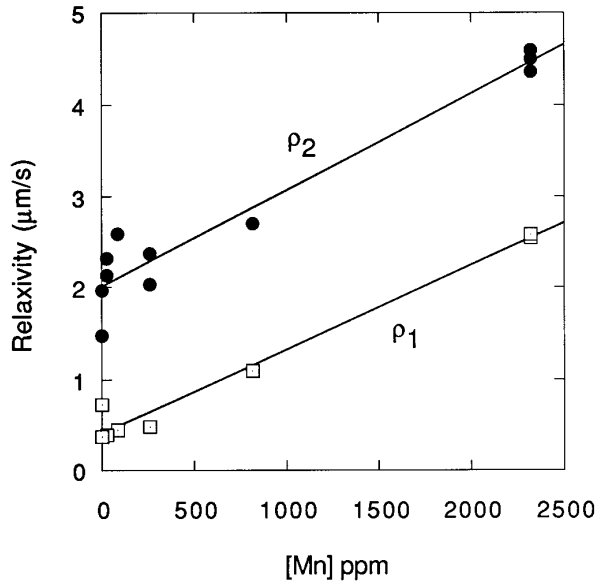

FIG. 4. Longitudinal (open squares) and transverse (solid circles) surface relaxivities for the manganese-doped materials. The straight lines are least-squares fits to the data.

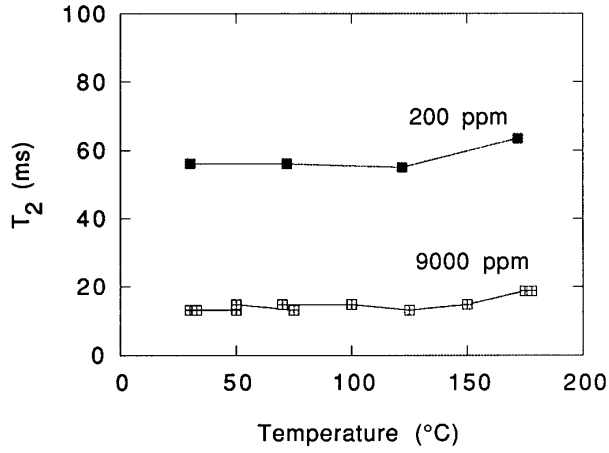

FIG. 5. The temperature dependence of the transverse relaxation time for samples with low and high concentrations of iron.

Note that the relaxivities of the iron and manganese series extrapolate to different values at zero dopant concentration. This apparent paradox is discussed below.

The temperature dependence of T_2 of two iron-doped samples is shown in Fig. 5. There is little or no effect of temperature. According to the theory of Kleinberg *et al.* (*3*), this observation eliminates from consideration any relaxation mechanisms that depend on diffusion, molecular motion, or the residence time of the fluid molecule on the surface. Such processes are thermally activated, and so are expected to have large temperature dependences. This is consistent with the linear dependence of the relaxivity on paramagnetic ion concentration: relaxation must be controlled by temperature-independent magnetic interactions at the surface, across the full range of paramagnetic ion concentrations.

The ratio of longitudinal to transverse relaxation times for the iron-bearing samples is shown in Fig. 6. It increases monotonically but not linearly with paramagnetic ion concentration. T_1/T_2 must be greater than unity, and in the context of the paramagnetic relaxation theory presented above should be greater than 7/6. This condition is satisfied except for the sample with the lowest paramagnetic ion content. The values are in the range that has been observed in sedimentary rocks (*34*).

DISCUSSION

For the purposes of estimating the principal parameters of the theory, we simplify Eqs. [5] and [6] by assuming that $\omega_I\tau_{c1} \ll 1$, and $\omega_s\tau_{c2} \gg 1$ or $\tau_{c1} \gg \tau_{c2}$, which will be justified below. The longitudinal surface relaxivity is

$$\rho_1 = \frac{n_M h}{T_{1M}} \qquad [26]$$

$$\frac{\Delta\rho_1}{\Delta n_M} = h\,\frac{6}{15}\left(\frac{\alpha A_d}{\hbar}\right)^2 S(S+1)\tau_{s1} \qquad [27]$$

and the ratio of the slopes on a relaxivity-composition plot is

$$\frac{\Delta\rho_2/\Delta n_M}{\Delta\rho_1/\Delta n_M} = \frac{7}{6} + \frac{5}{6}\left(\frac{A_s}{\alpha A_d}\right)^2. \qquad [28]$$

The following quantities are unknown: (1) h, the thickness of the layer of water at the fluid–solid interface; (2) α, the molecular-rotational anisotropy factor; (3) r, the metal–proton distance, which is the only unknown parameter in A_d; (4) A_s, the scalar coupling constant; and (5) τ_{s1}, the electron longitudinal relaxation time.

Somewhat arbitrarily, we shall assume values for three of the parameters and determine the other two from the data. We assume that $h = 3.5 \times 10^{-8}$ cm, the diameter of the water molecule; $\alpha = 1$, since α must be of the order of unity; and $r = 2.9 \times 10^{-8}$ cm, the metal–proton distance in aqueous solutions of both iron and manganese (*15*). Therefore the dipolar coupling constant A_d is the same for iron and manganese since they have the same value of g (*35*). We find that $\tau_{s1} = 0.8$ ns for both ions, and $A_s/h = 4.5$ MHz for iron and $A_s/h = 0$ for manganese. These compare to the corresponding solution values of 1.2 MHz for iron and 0.6–1.0 MHz for manganese (*15*).

We now must assess the adequacy of the assumptions that were used to derive Eqs. [27] and [28]. We have established

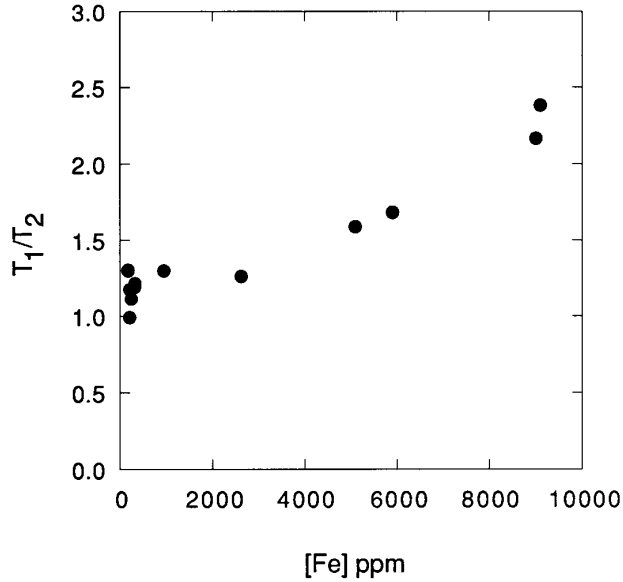

FIG. 6. The ratio of relaxation times versus concentration for the iron-doped samples.

that the correlation times in Eqs. [8] and [9] are dominated by the electron relaxation times τ_{s1} and τ_{s2}, respectively. The measurements were performed at a proton resonance frequency $\omega_I/2\pi = 2$ MHz. For $S = \frac{5}{2}$ ions, g is normally equal to its free-electron value (*35*), so $\omega_s/\omega_I = 658$. In many cases the ESR linewidth of transition metal ions is dominated by lifetime broadening (*35*), which implies that τ_{s1} is approximately equal to τ_{s2}, and therefore $\omega_I\tau_{c1} = 0.01$ and $\omega_s\tau_{c2} = 7$. The alternative is that $\tau_{s1} > \tau_{s2}$. As long as τ_{s1} is equal to either τ_{s2} or at least an order of magnitude larger than it, the assumptions used to derive Eqs. [27] and [28] are satisfied.

The relatively large value of relaxivity when the paramagnetic ion concentration is extrapolated to zero is surprising. The observed relaxivity in the limit $[M] = 0$ is probably not due to slowed rotation of water adsorbed on the solid surface. Let us make the usual assumption that in the absence of a paramagnetic center, the strongest magnetic interaction experienced by a proton in a water molecule is due to the intramolecular and intermolecular dipole–dipole coupling with other protons. Then T_1 is a minimum when the motional correlation time of the water molecule is approximately equal to the proton Larmor frequency. When that condition is satisfied (*14*)

$$T_{1\min} = \frac{1.05\omega}{\gamma_I^2\langle\Delta H^2\rangle}, \qquad [29]$$

where $\langle\Delta H^2\rangle$ is the second moment of the proton–proton dipolar interaction (*14*):

$$\langle\Delta H^2\rangle = \frac{1}{N}\sum_{i=1}^{N}\frac{9}{20}\gamma_I^2\hbar^2\sum_{k\neq i}^{N}\left(\frac{1}{r_{ik}}\right)^6. \qquad [30]$$

For ice, the proton second moment has the value (*36*) $\langle\Delta H^2\rangle = 32.1\ \mathrm{G}^2$, which is surely an overestimate of the dipolar interactions a water molecule might experience on a calcium silicate surface. Thus at 2 MHz, $T_{1\min} = 5.7 \times 10^{-4}$ s, so for a surface layer thickness $h = 3.5 \times 10^{-8}$ cm, the surface relaxivity can be no larger than 0.6 μm/s. This is considerably smaller than the observed value of approximately 3 μm/s found for the iron series. However, this upper bound is consistent with the zero-concentration intercept of the manganese ρ_1 data. We note that at 10 MHz, $\rho_{1\max} = 0.1$ μm/s, which is substantially lower than the value Kenyon and Kolleeny (*21*) found for very pure calcium carbonate.

The lack of temperature dependence of relaxation time at negligible paramagnetic ion concentrations further indicates that even in this limit the relaxation mechanism is paramagnetic in nature. A point defect is formed when an atom is lost from a solid surface. Such defects are known to be relatively common on oxide surfaces (*37*). These defects can be populated by localized unpaired electron spins which are paramagnetic sites (*35*). Paramagnetic defect sites, F centers and V centers, have been studied extensively in bulk solids by electron spin resonance. It is probably not possible to study analogous sites on the surface of micrometer-sized particles by the same means because the ESR signal from the surface would be overwhelmed by the signal from the bulk. Electron spins resident on the solid surface are perhaps most sensitively probed by the hyperfine-enhanced magnetic relaxation rate of fluid protons.

We hypothesize, but cannot prove, that paramagnetic crystal-defect sites exist in sufficient abundance on pseudowollastonite surfaces to explain the observed relaxation values. If the value of τ_{s1}/r^6 for such sites were the same as that of iron, then they would exist at a concentration of order 10^3 ppm. However, since free-electron relaxation times are usually quite long, it is very likely that their population is much smaller than this estimate would indicate.

The paramagnetic defect model may explain why the $Mn\cdot CaSiO_3$ series has a different relaxivity at $[Mn] = 0$ than the $Fe\cdot CaSiO_3$ series has at $[Fe] = 0$. Whereas the iron series was synthesized at 1400°C under oxidizing conditions, the manganese series was synthesized under nitrogen. This makes it likely that the number and kind of defects are substantially different in the two series.

CONCLUSIONS

The results of this investigation lend confidence to the hypothesis that the oxide surface of pseudowollastonite is a good model of the oxide surface of sandstones, when investigating the NMR properties of fluids in porous media. The T_1/T_2 ratios found here coincide with the values observed in rock studies. Lack of temperature dependence is further evidence of correspondence between the pseudowollastonite materials and natural rocks. For the relaxation times of fluids in porous media to be independent of temperature, all of the following conditions must be satisfied: (1) magnetic relaxation of fluid protons must be limited by the rate of relaxation at the surface, not by the rate of molecular diffusion to the surface; (2) relaxation at the surface cannot be dominated by any thermally activated process, such as adsorption, motion along the surface, or slowed molecular rotation at the surface; and (3) the electron relaxation times must be independent of temperature over the temperature range investigated. All these conditions are evidently satisfied in both natural rocks and the synthetic materials studied here, over the entire ranges of temperature and composition investigated.

From the standpoint of understanding the NMR properties of fluids in rocks, it is very encouraging to see that the ranges of ρ_1 and ρ_2 found in this study overlap measurements of surface relaxivity of rocks (*38, 39*). They also are consistent with the consensus value of ρ_2 derived from comparisons of

NMR relaxation time with capillary pressure measurements based on mercury porosimetry and water desaturation techniques (*6*). This is true even though the materials studied here are completely devoid of clay or other high-surface-area minerals, while sandstones have a large clay content. This tends to substantiate the hypothesis (*6*) that, despite its very large BET surface area, clay does not play a role in the relaxation of water in the bodies of sandstone pores. Clay-bound water does not mix with pore water, but relaxes independently of it, and therefore occupies a distinct range in the T_2 distribution.

It is also noteworthy that over the entire range of iron concentrations, ρ_2 varies only by a factor of six. This may explain the heretofore surprising success of the correlation of NMR relaxation time with hydraulic permeability (*33*). This correlation depends on the relative constancy of the surface relaxation in a wide variety of sandstones, which have a significant range of iron concentrations and clay contents. Figure 3 appears to resolve a long-standing mystery.

ACKNOWLEDGMENTS

Drs. T. Jones, W. Halperin, and P. West offered valued advice on the use of cementitious materials in this investigation. The materials were synthesized under the direction of Dr. West. We benefited from discussions with Drs. S. Greenbaum, D. Woessner, C. Straley, and M. Hurlimann on NMR and ESR technique and interpretation. I.F. thanks Dr. Greenbaum and Dr. R. Marino for encouragement and guidance.

REFERENCES

1. F. Bloch, *Phys. Rev.* **83,** 1062 (1951).
2. J. Korringa, D. O. Seevers, and H. C. Torrey, *Phys. Rev.* **127,** 1143 (1962).
3. R. L. Kleinberg, W. E. Kenyon, and P. P. Mitra, *J. Magn. Reson. A* **108,** 206 (1994).
4. K. F. Clark, *in* ''Handbook of Physical Properties of Rocks'' (R. S. Carmichael, Ed.), Vol. 1, Chap. 1, CRC Press, Boca Raton, Florida, 1982.
5. G. Sposito, ''The Surface Chemistry of Soils,'' Oxford Univ. Press, London, 1984.
6. R. L. Kleinberg, *Magn. Reson. Imaging,* in press.
7. W. E. Kenyon, *Nucl. Geophys.* **6,** 153 (1992).
8. R. L. Kleinberg, Well digging, *in* ''Encyclopedia of Nuclear Magnetic Resonance,'' Wiley, New York, 1996.
9. Z. Taicher, G. Coates, Y. Gitartz, and L. Berman, *Magn. Reson. Imaging* **12,** 285 (1994).
10. R. L. Kleinberg, A. Sezginer, D. D. Griffin, and M. Fukuhara, *J. Magn. Reson.* **97,** 466 (1992).
11. R. J. S. Brown and I. Fatt, *Pet. Trans. AIME* **207,** 262 (1956).
12. K. R. Brownstein and C. E. Tarr, *Phys. Rev. A* **19,** 2446 (1979).
13. L. L. Latour, R. L. Kleinberg, and A. Sezginer, *J. Colloid Interface Sci.* **150,** 535 (1992).
14. H. Pfeifer, *in* ''NMR: Basic Principles and Progress'' (P. Diehl *et al.,* Eds.), Springer-Verlag, New York, 1972.
15. I. Bertini and C. Luchinat, ''NMR of Paramagnetic Molecules in Biological Systems,'' Benjamin/Cummings, Menlo Park, California, 1986.
16. M. Rubinstein, A. Baram, and Z. Luz, *Mol. Phys.* **20,** 67 (1971).
17. W. P. Halperin, F. D'Orazio, S. Bhattacharja, and J. C. Tarczon, *in* ''Molecular Dynamics in Restricted Geometries'' (J. Klafter and J. M. Drake, Eds.), Chap. 11, Wiley, New York, 1989.
18. G. C. Borgia, R. J. S. Brown, P. Fantazzini, E. Mesini, and G. Valdre, *Nuovo Cimento* **14D,** 745 (1992).
19. K. R. McCall, D. L. Johnson, and R. A. Guyer, *Phys. Rev. B* **44,** 7344 (1991).
20. L. L. Latour, R. L. Kleinberg, P. P. Mitra, and C. H. Sotak, *J. Magn. Reson. A* **112,** 83 (1995).
21. W. E. Kenyon and J. A. Kolleeny, *J. Colloid Interface Sci.* **170,** 502 (1995).
22. F. A. Cotton and G. Wilkinson, ''Advanced Inorganic Chemistry,'' Chap. 19, Interscience, New York, 1972.
23. R. C. Weast and M. J. Astle (Eds.), ''CRC Handbook of Chemistry and Physics,'' 63rd ed., CRC Press, Boca Raton, Florida, 1982.
24. S. Lowell and J. E. Shields, ''Powder Surface Area and Porosity,'' Chapman & Hall, New York, 1984.
25. A. Sezginer, R. L. Kleinberg, M. Fukuhara, and L. L. Latour, *J. Magn. Reson.* **92,** 504 (1991).
26. C. L. Vavra, J. G. Kaldi, and R. M. Sneider, *Am. Assoc. Petrol. Geol. Bull.* **76,** 840 (1992).
27. D. P. Gallegos and D. M. Smith, *J. Colloid Interface Sci.* **122,** 143 (1988).
28. S. W. Provencher, *Comput. Phys. Commun.* **27,** 213 (1982).
29. M. G. Prammer, Soc. Petrol. Eng. Paper No. 28368 (1994).
30. R. Freedman, U.S. Patent 5,291,137 (1994).
31. E. J. Fordham, A. Sezginer, and L. D. Hall, *J. Magn. Reson. A* **113,** 139 (1995).
32. C. Straley and L. M. Schwartz, *Magn. Reson. Imaging,* in press.
33. W. E. Kenyon, P. I. Day, C. Straley, and J. F. Willemsen, *Soc. Petrol. Eng. Form. Eval.* **3,** 622 (1988); erratum: *Soc. Petrol. Eng. Form. Eval.* **4,** 8 (1989).
34. R. L. Kleinberg, S. A. Farooqui, and M. A. Horsfield, *J. Colloid Interface Sci.* **158,** 195 (1993).
35. J. E. Wertz and J. R. Bolton, ''Electron Spin Resonance,'' McGraw–Hill, New York, 1972.
36. J. A. Glasel, *in* ''Water, a Comprehensive Treatise'' (F. Franks, Ed.), Vol. 1, Chap. 6, Plenum, New York, 1972.
37. V. E. Henrich and P. A. Cox, ''The Surface Science of Metal Oxides,'' Cambridge Univ. Press, London, 1994.
38. M. D. Hurlimann, K. G. Helmer, L. L. Latour, and C. H. Sotak, *J. Magn. Reson. A* **111,** 169 (1994).
39. G. C. Borgia, R. J. S. Brown, and P. Fantazzini, *J. Appl. Phys.* **79,** 3656 (1996).